HHS Public Access

Author manuscript

Neurobiol Aging. Author manuscript; available in PMC 2016 November 01.

Published in final edited form as:

Neurobiol Aging. 2015 November ; 36(11): 2963–2971. doi:10.1016/j.neurobiolaging.2015.07.016.

Matrix Metalloproteinase 9 mediated intracerebral hemorrhage induced by Cerebral amyloid angiopathy

Lingzhi Zhao, PhD[a], **Michal Arbel-Ornath, PhD**[a], **Xueying Wang, PhD**[a], **Rebecca A. Betensky, PhD**[b], **Steven M. Greenberg, MD, PhD**[a], **Matthew P. Frosch, MD, PhD**[a,c], and **Brian J. Bacskai, PhD**[a,*]

[a]Department of Neurology/Alzheimer Research Unit, Massachusetts General Hospital, Charlestown, Massachusetts 02129

[b]Department of Biostatistics, Harvard School of Public Health, Boston, Massachusetts 02115

[c]C.S. Kubik Laboratory of Neuropathology, Department of Pathology, Massachusetts General Hospital, Boston, Massachusetts 02114

Abstract

Cerebral amyloid angiopathy (CAA), the deposition of β-amyloid (Aβ) in cerebrovascular walls, is the most common cause of lobar hemorrhagic stroke. Previous studies show that cerebrovascular Aβ induces expression and activation of matrix metalloproteinase 9 (MMP-9) in cerebral vessels of amyloid precursor protein (APP) transgenic mice. Here we extended these findings and evaluated MMP-9 expression in postmortem brain tissues of human CAA cases. MMP-9 co-localized with CAA, correlated with the severity of the vascular pathology, and was detected in proximity to microbleeds. We characterized a novel assay using longitudinal multi-photon microscopy and a novel tracer to visualize and quantify the magnitude and kinetics of hemorrhages in 3-dimensions in living mouse brains. We demonstrated that topical application of recombinant MMP-9 resulted in a time- and dose-dependent cerebral hemorrhage. APP mice with significant CAA developed more extensive hemorrhages which also appeared sooner after exposure to MMP-9. Our data suggest an important role for MMP-9 in development of hemorrhages in the setting of CAA. Inhibition of MMP-9 may present a preventive strategy for CAA-associated hemorrhage.

Keywords

Cerebral amyloid angiopathy (CAA); Matrix Metalloproteinase (MMP); intracerebral hemorrhage; multi-photon microscopy; amyloid-β

*Corresponding author: Brian J. Bacskai, PhD, Massachusetts General Hospital, 114 16th St., Charlestown, MA 02129, Tel: (617) 724-5306, Fax: (617) 724-1480, bbacskai@partners.org.

Disclosure statement

The authors have no actual or potential conflicts of interest.

1. Introduction

Cerebral amyloid angiopathy (CAA) is the deposition of β-amyloid (Aβ) primarily in cerebral arteries and is present in 10–40% of general autopsies and ≥ 80% of cases of Alzheimer disease (AD) (Glenner and Wong, 1984; Jellinger, 2002; Okazaki et al., 1979; Vinters, 1987). CAA is often found accompanied with lobar hemorrhages and cerebral infarcts and is believed to be the most common cause of lobar hemorrhagic stroke (Greenberg, 1998; Greenberg and Vonsattel, 1997; Jellinger, 2002; Mandybur, 1986; Okazaki et al., 1979; Vonsattel et al., 1991). Unlike nearly all other causes of stroke, little is known about the molecular pathogenesis of CAA and currently no preventive treatment is available. Accumulation of Aβ in vessel walls induces many vasculopathic abnormalities, such as vessel wall thickening, luminal narrowing, hypoperfusion, vascular smooth muscle cells (VSMC) degeneration, and inflammation (Cadavid et al., 2000; Greenberg, 1998; Greenberg and Vonsattel, 1997; Jellinger, 2002; Mandybur, 1986; Vinters, 1987; Vonsattel et al., 1991). However, the deposition of Aβ is not sufficient for destruction of cerebrovascular integrity, which suggests that additional destructive mechanisms are likely involved in the basement membrane breakdown or the injury of the vessel walls.

One class of molecules that may participate in the regulation of vascular integrity are the matrix metalloproteinases (MMPs). MMPs are a family of 23 zinc-dependent endopeptidases capable of degrading virtually all of the components constituting basement membranes and connective tissue. MMPs are therefore assumed to play an essential role in the homeostasis of the extracellular matrix and vascular integrity (Florczak-Rzepka et al., 2012; Lakhan et al., 2013; Okazaki et al., 1979; Seo et al., 2012). Matrix metalloproteinase-9 (MMP-9; gelatinase B) has received considerable attention due to its involvement in a variety of vasculopathies and hemorrhagic transformation after cerebral ischemia (Asahi et al., 2001; Cui et al., 2012; Lakhan et al., 2013; McColl et al., 2010; Ramos-Fernandez et al., 2011). Elevated MMP-9 immunoreactivity has been reported to be spatially associated with microbleeds in a mouse model of CAA (Lee et al., 2003), although the irrelevance of MMP-9 with CAA-related vascular dysfunction has also been reported (Hernandez-Guillamon et al., 2012). MMP-9 is widely expressed in all vascular unit cell types such as endothelial cells, VSMC, astrocytes, microglia, pericytes, and macrophages. Previous studies have demonstrated that Aβ induces the synthesis, release and activation of matrix MMP-9 in cultures of these cell types (Gottschall, 1996; Guo et al., 2006; Hartz et al., 2012; Lee et al., 2003; Wang et al., 2002; Zhao et al., 2009), suggesting that Aβ may boost the effects of MMP-9 on vascular disruption. Further studies may therefore be needed to understand the pathological significance of MMP-9 in CAA and CAA-associated vascular dysfunctions.

In this report, we characterized the expression of MMP-9 in vessels of postmortem human brain tissue from CAA patients and correlated its levels with the severity of CAA. Based on these results, we established a quantitative *in vivo* hemorrhage assay that can visualize and quantify the magnitude of hemorrhage using multi-photon microscopy and a new tracer. We applied this assay to determine whether MMP-9 interacts with Aβ to exaggerate the vascular abnormalities and ICH occurrence in mice. This work demonstrated that MMP-9 can trigger vascular leakage and ICH; it may act with Aβ in a synergistic way to disrupt vascular

integrity, suggesting that manipulation of MMP-9 may delineate a potential therapeutic target to prevent CAA associated hemorrhage.

2. Materials and Methods

2.1. Animals and reagents

C57/BL6 mice (male, 3 to 4 months old) were obtained from Charles River Laboratories. Tg2576 mice (expressing human Swedish mutation of APP. Male, 12 to 14 months old) and their aged-matched non-transgenic littermates were bred and aged in house. All animal studies were in compliance with the Massachusetts General Hospital Animal Care and Use Committee and National Institutes of Health guidelines. MMP-9 antibody (catalytic domain) and anti-glial fibrillary acidic protein (GFAP) antibody were purchased from Millipore; recombinant human MMP-9 (pre-activated) was purchased from Anaspec; monoclonal antibody against human fibrin (a′-fibrin) was purchased from American Diagnostic Inc.; The anti-fibrin antibody was labeled with DyLight 594 using a commercial kit (Thermo Scientific); Prussian blue staining kits were purchased from Polysciences, Inc.

2.2. Brain specimens

Formalin-fixed paraffin-embedded brain tissues were obtained from the occipital lobe of 10 patients diagnosed with CAA or AD combined with CAA. Sections from 5 non-demented age-matched individuals were used as controls. The neuropathologies of each case were assessed according to the ABC scoring scheme (Montine et al., 2012) (Table 1). Five of the 10 cases with moderate to severe CAA had symptomatic lobar hemorrhages. (4 of the 6 CAA cases, and 1 of the CAA+AD cases.) All cases were from the Neuropathology Core of the Massachusetts Alzheimer Disease Research Center Brain Bank, and the study protocol was approved by the Institutional Review Board.

2.3. Severity of CAA

CAA in human tissue samples was graded with respect to the severity of the pathology as previously described with minor modifications (Greenberg and Vonsattel, 1997; Vonsattel et al., 1991). Using 0–4 scoring system, a “0” indicates no Aβ positive blood vessels. A “1” is scattered Aβ positivity in either leptomeningeal or intracortical blood vessels. A score of “2” indicates strong, circumferential Aβ positivity in either some leptomeningeal or intracortical blood vessels. A “3” reflects full replacement of the vessel wall with amyloid plus partial or full cracking of vessel wall in leptomeningeal and intracortical blood vessels. A score of “4” is the same as 3 with additional dysphoric changes. Advanced grade 3 or grade 4 CAA-affected vessels demonstrate a “vessel-within-vessel” lumen, suggestive of a weakened vascular extracellular matrix (ECM) resulting in the separation of intima from media during tissue preparation (Mandybur, 1986; Vonsattel et al., 1991).

2.4. Immunohistochemistry

Staining was performed as previously described (Serrano-Pozo et al., 2013). Briefly, postmortem human brain sections (5 μm/section, four sections per case) were cleared in xylenes, rehydrated with decreasing concentrations of ethanol, and subjected to a standard antigen-retrieval procedure consisting of a 20-minute boiling in citrate buffer (0.01 M, pH

6.0) with 0.05% Tween 20. The sections were cooled at 4 °C for 30 t o 45 minutes, blocked with 5% normal goat serum at room temperature for one hour, and incubated with anti-MMP-9 antibody (1:200) or anti-GFAP antibody (1:1000) overnight at 4 °C. The next day, the sections were washed three times (10 minutes for each wash) with Tris-Buffered Saline (TBS), incubated with the fluorescence conjugated secondary antibodies or processed with a vectastain ABC Elite kit (Vecto) and 3, 3′-diaminobenzidine (DAB) solution (DAB staining). Hematoxylin counterstaining was performed in DAB sections if needed. Negative controls were obtained by omitting the primary antibodies. Hematoxylin and eosin (H&E), thioflavin S, and Prussian blue staining were performed according to standard protocols. Images were taken with either an epifluorescence microscope (Olympus, BX61) or a confocal microscope (Zeiss, LSM510). For counting thioflavin S positive or MMP-9 positive vessels, four sections from each case, 50 μm apart, were stained with thioflavin S and an anti-MMP-9 antibody. Two hundred vessels per section (800 vessels in total from each case) were randomly selected by the CAST stereology software to count the numbers of vessels with or without immunoreactivity to MMP-9 or thioflavin S. This stereology software ensures an unbiased sampling of all sections.

2.5. Craniotomy surgery

Craniotomy surgery was performed as previously described (Skoch et al., 2005). Briefly, animals were anesthetized using isoflurane (1.5%), the skin and periosteum were removed and a 6-mm diameter craniotomy was performed, making the anterior end immediately anterior to bregma and the posterior end just anterior to lambda. After removing the dura mater, a coverslip was attached over the cranial window site and the animals were imaged with a multiphoton imaging system (Fluoview 1000MPE, Olympus, USA). A fluorescent tracer was intravenously injected in a lateral tail vein of each mouse to provide a fluorescent angiogram.

2.6. Multiphoton microscopy

Multiphoton imaging and processing was performed as previously described with modifications (Klunk et al., 2002; Skoch et al., 2005). Briefly, a wax ring was built on the edge of the cranial window to create a well of water for the objective (Olympus XLPlan N 25X, numerical aperture 1.05). After craniotomy surgeries, mice were imaged immediately to acquire the background images. The coverslips were removed; PBS or recombinant MMP-9 was applied at a final volume of 30 μl in a range of concentrations as indicated in the Results. The windows were tightly fixed with dental cement. The animals were infused with 200 μl (100 μg) of a fluorescent tracer (DyLight 594-conjugated anti-fibrin antibody, DyLight 594-PHF1, Texas Red-conjugated dextran 70 kDa, or fluorescein isothiocyanate-conjugated dextran 70 kDa) via tail vein and immediately imaged at baseline (time 0h) followed by imaging hourly using the Olympus FluoView FV1000MPE multiphoton laser-scanning system mounted on an Olympus BX61WI microscope (Olympus). A Ti:sapphire mode-locked laser (DeepSee Mai Tai; Spectra-Physics) generated two-photon fluorescence with 800 nm excitation. Emitted light was detected through three filters in the range of 420–460, 495–540, and 575–630 nm. Blood vessels were imaged with 3 μm/section (512 × 512; z-step: 3 μm, up to 200 μm) hourly up to 7 hours. Thirty minutes before imaging at the 7 hour time point, 300 μl of methoxy-X04 was intraperitoneally injected into the animal to

label CAA-affected vessels (Klunk et al., 2002). MMP-9-induced bleeding was visualized by detection of the fluorescence signals of tracers leaking from vessels in bran parenchyma. Images were projected as sum intensity. The fluorescence intensity of DyLight 594-anti-fibrin in sum intensity projection of stacks was analyzed using ImageJ software.

2.7. Statistical analysis

Statistical analysis was performed using Student's *t* test and two-way ANOVA provided in the OriginLab Origin 8 graphics and statistics software. Values of $p < 0.05$ were considered significant. A conditional logistic regression model for the MMP-9 outcome that was stratified by patients was used to adjust for correlation of MMP-9 within patients, and to test for an interaction between thioflavin S staining and disease category on MMP-9 intensity. For correlations between MMP-9 intensity and CAA severity, a linear mixed effects model with a random effect for patient and fixed effects for CAA stage of vessels and disease category was used.

3. Results

3.1. MMP-9 accumulates in CAA vessels in a CAA severity dependent manner

To systematically assess the contribution of MMP-9 to human CAA pathogenesis, brain sections (four sections from each case, 50 μm apart) from the occipital lobes of 10 patients diagnosed with CAA or AD combined with CAA were examined by staining with an antibody recognizing the catabolic domain of MMP-9. CAA affected vessels were identified by thioflavin S staining. As shown in Fig. 1, the immunoreactivity of MMP-9 was observed primarily in tunica media and around Aβ-compromised vessels in advanced CAA. In contrast, no MMP-9 immunoreactivity was detected in brain sections from control subjects (Fig. 1A). The number of vessels (800 vessels per case) with or without immunoreactivity of MMP-9 or thioflavin S was quantified, as shown in Fig. 1B, 78.9 ± 23.9% of vessels that were positive for MMP-9 were also positive for thioflavin S staining. In contrast, the expression of MMP-9 was undetectable in 95.3 ± 1.3% of thioflavin S negative vessels (non-CAA vessels) across all disease states (data not shown), indicating a close association of MMP-9 with CAA pathogenesis.

To further define the spatial and temporal contribution of MMP-9 to CAA progression, vessels in all examined cases were divided into four groups according to the severity of CAA. The immunoreactivity of MMP-9 in vessels at different stages was quantified. As shown in Fig. 1C and D, the expression of MMP-9 was significantly increased in CAA vessels at late stages (stage 3 and stage 4) compared to that at early stages (stage 0 and stage 1). No statistical difference in MMP-9 expression was observed between CAA vessels at stage 0 and unaffected vessels in age-matched controls, suggesting that the effect of amyloid on MMP-9 expression is spatially restricted. Double staining of brain sections with antibodies recognizing MMP-9 and an astrocytic marker glial fibrillary acidic protein (GFAP) revealed a spatial association of MMP-9 with the end feet of astrocytes (Supplemental 1A, B).

Spontaneous intracerebral hemorrhage (ICH) is the most frequent and severe clinical manifestation of advanced CAA (Vonsattel et al., 1991). Given the capability of MMP-9 to

digest proteins that compose basement membranes and connective tissue, we next examined whether MMP-9 is associated with CAA-related hemorrhage. The bleeds in the parenchyma of human brain tissues were examined by Prussian blue staining, which recognizes the iron from extravasated blood due to hemorrhage. As shown in Fig. 1E, Prussian blue positive products were primarily observed in areas with a cluster of vessels showing strong immunoreactivities of MMP-9, suggesting a potential contribution of MMP-9 to CAA-related ICH.

3.2. MMP-9 induces hemorrhage *in vivo*

Given the association of MMP with CAA and ICH that we observed in human tissue, we attempted to model the role of MMP-9 in induction of hemorrhage in mice. C57/BL6 mice at 3 months of age were prepared with a craniotomy followed by careful removal of dura mater. Recombinant MMP-9 (rMMP-9, 0.4 μg) containing the catabolic domain was pre-activated and topically applied to the surface of mouse brains. Forty eight hours after the treatment, the mice were sacrificed, and mouse brains were removed to examine the lobar hemorrhage under a low magnification microscope. As shown in Fig. 2A, profound lobar hemorrhage was observed in mouse brains treated with rMMP-9, but not in mouse brains treated with PBS. Mouse brains were further sectioned and processed for histologic examination by H&E staining. As shown in Fig. 2B, vascular rupture was only observed in mouse brains treated with rMMP-9, but not in mouse brains treated with PBS. Importantly, the hemorrhage induction activity of rMMP-9 was completely eliminated by heating rMMP-9 to 90°C for 30 minutes (Supplementary Fig. 2), indicating a causative role of MMP-9 in hemorrhage induction *in vivo*.

3.3. Real-time visualization and quantitation of lobar hemorrhage *in vivo* by multi-photon microscopy

To appreciate the kinetics of MMP-9-induced ICH with higher spatial and temporal resolution, we developed a novel method to detect bleeding based on intravenous injection of fluorescence-conjugated macromolecules that can be followed using multi-photon microscopy. The compromise of the blood-brain barrier can be assessed by detection of these fluorescent compounds in brain parenchyma. High molecular weight dextrans (such as dextran 70kDa) are commonly used tracers in investigation of vascular permeability; however, the signal of fluorescent dextrans is difficult to measure quantitatively because of the diffusion and clearance of these tracers (Arbel-Ornath et al., 2013). Therefore, to quantitatively measure the magnitude and the spatio-temporal pattern of hemorrhage, we employed a novel tracer using fluorescence-conjugated anti-fibrin antibodies. Fibrin is an insoluble protein that is an endogenous product in response to bleeding in the clotting reaction. When hemorrhage occurs, anti-fibrin antibody leaks into brain parenchyma with blood. Unlike other blood pool tracers which rapidly enter the interstitial space after compromise of the blood-brain barrier, the anti-fibrin antibody binds to fibrin at the site of clots and accumulates in proportion to the magnitude of the hemorrhage. Using intravital imaging of mouse brains, we tracked the fluorescent signal in real time and quantified the extent of hemorrhages based on fluorescence intensity and volume.

To characterize the efficiency of the fluorescence-conjugated anti-fibrin tracer in detection of vascular leakage, DyLight 594-labeled anti-fibrin antibody and Texas Red-dextran (70 kDa) were intravenously infused into the tail veins of C57BL6 mice that were topically administered 0.4 μg of rMMP-9. Both fluorescence signals were examined simultaneously in different channels with multi-photon imaging. As shown in Fig. 3A, when using fluorescent-labeled anti-fibrin tracer, in addition to the diffuse fluorescence signals, clots (recognized by the binding of the anti-fibrin antibody) were identified in brain parenchyma four hours after treatment with rMMP-9 (Fig. 3A, upper panel). In contrast, only diffuse Texas Red-dextran (70 kDa) was observed in brain parenchyma of the same mice (Fig. 3A, middle panel).

PHF1 is an antibody that recognizes the phosphorylated microtubule-associated protein tau, which is absent in the brains and blood of C57/BL6 mice. To test the specificity of fluorescent-anti-fibrin tracer in detection of a hemorrhage, fluorescent-labeled anti-fibrin or fluorescent-labeled PHF1 was intravenously injected via tail veins in C57/BL6 mice that topically treated with 0.4 μg of rMMP-9. The vascular leakage and clots in the mouse brains were imaged hourly using a multi-photon microscope. As shown in Fig. 3B and C, there was a time-dependent accumulation of fluorescence clots in mouse brains treated with rMMP-9 while using the fluorescent-anti-fibrin tracer (Fig. 3B, lower panel). In contrast, only diffuse fluorescence signals were observed, indicating a compromised blood-brain barrier, but no fluorescence signals resembling clots were detected over the entire course of the experiment in mouse brains with the same treatment using the fluorescent-PHF1 tracer (Fig. 3B, middle panel). As a control, no vascular leakage or ICH was observed in mice treated with PBS (Fig. 3B, upper panel).

Images were further analyzed quantitatively for the total volume of hemorrhage by determining the fluorescence intensity of fluorescent-anti-fibrin. As shown in Fig. 3D, higher concentration of rMMP-9 (0.2 μg or 0.4 μg) resulted in more rapid occurrence of ICH. Lower concentration of rMMP-9 (0.05 μg) failed to induce any detectable hemorrhage over the entire course of the experiment. Additionally, longer treatment with 0.4 μg of rMMP-9 resulted in a larger volume of hemorrhage (Fig. 3C).

3.4. Transgenic mice with CAA are more susceptible to MMP-9 induced hemorrhage

Tg2576 mice overexpress a mutant form of amyloid precursor protein (APP) bearing the Swedish mutation (KM670/671NL) (Hsiao et al., 1996). Tg2576 mice develop age-dependent Aβ deposits in brain parenchyma and the cerebral vasculature similar to that seen in humans with AD or CAA. By the age of ~15 months, Tg2576 mice develop severe CAA in leptomeningeal vessels. This mouse model is well characterized and has been used as a valuable tool to study the pathophysiological progression of CAA (Domnitz et al., 2005; Robbins et al., 2006).

We took advantage of our quantitative hemorrhage assay (as described above) to examine whether CAA vessels are more susceptible to MMP-9 induced bleeding. rMMP-9 (0.05 μg, a concentration that does not induce hemorrhage in wild type mice) was topically administered to 15~16-month old Tg2576 mice or age-matched littermates. The occurrence and severity of hemorrhage were determined by the quantitative hemorrhage assay. As shown in Fig. 4, in addition to the diffuse fluorescence signals, fluorescent clots were

detected as soon as four hours in brains of Tg2576 mice after topical treatment with 0.05 μg of rMMP-9 (Fig. 4A, middle panel). In contrast, no fluorescence clots were observed over the entire course of the experiment (seven hours) in brains of age-matched non-transgenic littermates with the same treatment (Fig. 4A, upper panel).

To control for the variation between animals, as well as the possible influence of surgical procedures in causing bleeding, craniotomies were performed in Tg2576 mice where the dura mater was removed only on right hemispheres. When rMMP-9 was topically applied to these mice, only the right hemispheres were exposed to rMMP-9 whereas the left hemispheres were sheltered from the rMMP-9 exposure by the dura mater. rMMP-9 (0.05 μg) was topically applied to these mice and the animals were imaged hourly to measure the fluorescence signal. As shown in Fig. 4A, the fluorescent clots were only detected on the dura-removed sides (right hemispheres) of the brain (Fig. 4A, middle panel). No detectable clots were observed on the dura-preserved sides (left hemispheres) of the brains over the entire course of the experiment (Fig. 4A, lower panel). Moreover, the fluorescence signals and fluorescent clots were detected earlier in brains of Tg2576 mice topically treated with 0.05 μg rMMP-9 than those in the brains of WT mice or in the brain hemispheres that were protected by an intact dura mater ($p < 0.001$) (Fig. 4B). Additionally, Tg2576 mice developed greater magnitude cerebral hemorrhages than age matched nontransgenic littermates or in animals where the hemisphere was covered by dura matter when treated with the same concentration of rMMP-9 (Fig. 4C).

4. Discussion

The elevation of MMP-9 immunoreactivity in amyloid-laden vessels of aged APPsw mice has been previously reported by Lee et al (Lee et al., 2003, 2005). Garcia-Alloza et al. confirmed the activation of this protease in living transgenic mouse brains using an *in situ* zyomography (Garcia-Alloza et al., 2009). In contrast, Hernandez-Guillamon, et al. showed that MMP-9 expression was absent in vessels at early stage of CAA and was restricted in isolated macrophages and neutrophils in severe stage of CAA vessels (Hernandez-Guillamon et al., 2012). Here, we characterized a correlation between MMP-9 expression and the severity of CAA by examining postmortem human brain tissues. Furthermore, the accumulated MMP-9 is associated with extravasated blood products from advanced CAA-affected vessels. Although the cross-sectional analysis did not establish whether the elevated MMP-9 functions as a causative contributor to CAA pathogenesis or only an accompanying pathological phenomenon in CAA progression, our results suggest a mechanistic link between MMP-9 and CAA progression.

Examination of postmortem brain tissue is a powerful technique to study neuropathology, but it only provides a single snapshot in time. In animal studies, commonly used approaches for detecting the vascular compromise or stroke include intravenous injections of colorimetric compounds such as Evans blue or fluorescence-conjugated macromolecules that do not normally cross blood-brain barrier (Belayev et al., 1996; Shyong et al., 2007; Stitt et al., 2000; Trichonas et al., 2010; Uyama et al., 1988); however, the sensitivity of these assays is low and also limited to single points in time. Real time detection in living animal models circumvents this limitation and allows quantitative examination of

pathophysiology over time. Intravital imaging with multiphoton microscopy in combination with a fluorescent tracer is one of these methods and has been used to monitor the progression of CAA to address underlying mechanisms (Domnitz et al., 2005; Hsiao et al., 1996; Kimchi et al., 2001). We advanced this useful methodology and designed a novel tracer (fluorescence-labeled anti-fibrin antibody) that is based on the physiological reaction of hemorrhage *in vivo*. Our results have shown that the new intravital imaging method employing a fluorescent-anti-fibrin tracer is more sensitive, specific, and importantly more quantitative than using other fluorescent tracers for hemorrhage detection, which can help to uncover mechanisms related to vascular compromise and intracerebral hemorrhage.

Using this novel assay, we were able to define a direct role of MMP-9 in hemorrhage induction. We observed two distinct phenomena: the first was a diffuse leak of plasma constituents into the brain parenchyma. This was detectable with both the labeled dextran and antibody. The second was overt bleeding that led to clot formation in the brain parenchyma labeled with the anti-fibrin antibody. It is not clear whether these two MMP-9-induced processes occur during human ICH, either in series or in parallel, and if they can occur distinct from one another. In our system of MMP-9 application, diffuse leakage precedes clot formation, suggesting that the two processes occur in series. It is further tempting to speculate that the diffuse leakage might reflect the vasogenic edema observed in inflammatory CAA (Kinnecom et al., 2007; Piazza et al., 2013) or anti-amyloid therapies performed in clinical trials (Nicoll et al., 2003; Pfeifer et al., 2002). We also found that vessels in APP-expressing transgenic mice show an earlier occurrence and greater magnitude of both diffuse leakage and ICH than wild type controls, suggesting an increased vulnerability of intracerebral vessels in the presence of CAA. One possible mediator of this effect might be an increased tonic level of MMP activation in the transgenic mouse brain. While the effects were not focally associated with CAA deposits on individual vessels, the presence of amyloid deposits in brains nonetheless appeared sufficient to increase the propensity to bleed. It is likely that soluble amyloids contribute to the susceptibility of hemorrhage in the older APP mice. We have not performed a systematic study to identify the effects of soluble Aβ or insoluble aggregates on CAA-related hemorrhage, but in trial experiments we did not observe an increase in susceptibility to bleeding in young APP transgenic mice. Because the concentration of amyloids are lower in younger mice in parallel with the reduced aggregated amyloid (plaques and CAA), it is challenging to decipher the contribution of soluble vs insoluble aggregates by only comparing young and old APP mice.

The integrity of connective tissues is determined by the delicate balance between the synthesis and degradation or desorption of extracellular matrix (ECM) molecules. An alteration of this balance is associated with a variety of pathological conditions (Baeten and Akassoglou, 2011). Additionally, the expression and activation of MMPs are regulated at several levels, including transcription, release, proenzyme activation, and interaction with endogenous tissue inhibitors of MMPs (TIMPs) or other MMP isoforms (Lakhan et al., 2013; Nagase and Woessner, 1999). Although we have described a close association of MMP-9 with CAA-associated hemorrhage, we cannot exclude these or other mechanisms involved in the compromised vascular integrity. Additionally, MMP-9 is widely expressed

in various CNS cells (such as astrocytes, microglia, neurons, et al.) and its expression in these cells can be markedly induced in response to Aβ exposure in AD brains. While we did not explore every cell type, we have found that astrocytes are recruited to the CAA-affected vessels and their end feet are closely associated with the expression of MMP-9, suggesting that astrocytes, especially at advanced stages, may serve as an important source of MMP-9 and may also be involved in MMP-9-mediated vascular permeability regulation. The role of other cells in MMP-9-associated CAA pathogenesis may be investigated in a future study. Furthermore, current available animal models of AD and/or CAA often resemble genetic but not sporadic forms of CAA. Genetic forms of CAA in humans are more aggressive and more frequently occur in the occipital lobes. New CAA animal models that can closely represent clinic pathogenesis may be required to clarify the role and mechanisms of MMPs in CAA progression.

In summary, our study combined the examination of postmortem human brain samples and the investigation of animal models using a new established technique. Our results indicate that MMP-9 is highly associated with CAA and CAA progression, induces hemorrhage *in vivo* and may be an important contributor for CAA-associated hemorrhage. Inhibition of MMP-9 activation may hence serve as a potential strategy to prevent and treat CAA and the CAA-associated vascular abnormalities.

Supplementary Material

Refer to Web version on PubMed Central for supplementary material.

Acknowledgments

The authors thank Dr. Peter Davies (The Feinstein Institute for Medical Research, Manhasset, NY) for providing the PHF1 antibody. Drs. Julia Gregory, Ksenia Kastanenka, and Alberto Serrano-Pozo (Massachusetts General Hospital, Boston, MA) for their valuable discussion and suggestions on the project. We also acknowledge support from grants NIH EB00768 and S10 RR025645.

References

Arbel-Ornath M, Hudry E, Eikermann-Haerter K, Hou S, Gregory JL, Zhao L, Betensky RA, Frosch MP, Greenberg SM, Bacskai BJ. Interstitial fluid drainage is impaired in ischemic stroke and Alzheimer's disease mouse models. Acta Neuropathol. 2013; 126:353–364. [PubMed: 23818064]

Asahi M, Wang X, Mori T, Sumii T, Jung JC, Moskowitz MA, Fini ME, Lo EH. Effects of matrix metalloproteinase-9 gene knock-out on the proteolysis of blood-brain barrier and white matter components after cerebral ischemia. J Neurosci. 2001; 21:7724–7732. [PubMed: 11567062]

Baeten KM, Akassoglou K. Extracellular matrix and matrix receptors in blood–brain barrier formation and stroke. 2011; 71:1018–1039.

Belayev L, Busto R, Zhao W, Ginsberg MD. Quantitative evaluation of blood-brain barrier permeability following middle cerebral artery occlusion in rats. Brain Res. 1996; 739:88–96. [PubMed: 8955928]

Cadavid D, Mena H, Koeller K, Frommelt RA. Cerebral beta amyloid angiopathy is a risk factor for cerebral ischemic infarction. A case control study in human brain biopsies. 2000; 59:768–773.

Cui J, Chen S, Zhang C, Meng F, Wu W, Hu R, Hadass O, Lehmidi T, Blair GJ, Lee M. Inhibition of MMP-9 by a selective gelatinase inhibitor protects neurovasculature from embolic focal cerebral ischemia. 2012; 7:21.

Domnitz SB, Robbins EM, Hoang AW, Garcia-Alloza M, Hyman BT, Rebeck GW, Greenberg SM, Bacskai BJ, Frosch MP. Progression of cerebral amyloid angiopathy in transgenic mouse models of Alzheimer disease. 2005; 64:588–594.

Florczak-Rzepka M, Grond-Ginsbach C, Montaner J, Steiner T. Matrix metalloproteinases in human spontaneous intracerebral hemorrhage: an update. Cerebrovasc Dis. 2012; 34:249–262. [PubMed: 23052179]

Garcia-Alloza M, Prada C, Lattarulo C, Fine S, Borrelli LA, Betensky R, Greenberg SM, Frosch MP, Bacskai BJ. Matrix metalloproteinase inhibition reduces oxidative stress associated with cerebral amyloid angiopathy *in vivo* in transgenic mice. J Neurochem. 2009; 109:1636–1647. [PubMed: 19457117]

Glenner GG, Wong CW. Alzheimer's disease: initial report of the purification and characterization of a novel cerebrovascular amyloid protein. Biochem Biophys Res Commun. 1984; 120:885–890. [PubMed: 6375662]

Gottschall PE. beta-Amyloid induction of gelatinase B secretion in cultured microglia: inhibition by dexamethasone and indomethacin. Neuroreport. 1996; 7:3077–3080. [PubMed: 9116244]

Greenberg SM. Cerebral amyloid angiopathy: prospects for clinical diagnosis and treatment. Neurology. 1998; 51:690–694. [PubMed: 9748011]

Greenberg SM, Vonsattel JP. Diagnosis of cerebral amyloid angiopathy. Sensitivity and specificity of cortical biopsy. Stroke. 1997; 28:1418–1422. [PubMed: 9227694]

Guo S, Wang S, Kim WJ, Lee S, Frosch MP, Bacskai BJ, Greenberg SM, Lo EH. Effects of apoE isoforms on beta-amyloid-induced matrix metalloproteinase-9 in rat astrocytes. Brain Res. 2006; 1111:222–226. [PubMed: 16919608]

Hartz AM, Bauer B, Soldner EL, Wolf A, Boy S, Backhaus R, Mihaljevic I, Bogdahn U, Klunemann HH, Schuierer G, Schlachetzki F. Amyloid-beta contributes to blood-brain barrier leakage in transgenic human amyloid precursor protein mice and in humans with cerebral amyloid angiopathy. Stroke. 2012; 43:514–523. [PubMed: 22116809]

Hernandez-Guillamon M, Martinez-Saez E, Delgado P, Domingues-Montanari S, Boada C, Penalba A, Boada M, Pagola J, Maisterra O, Rodriguez-Luna D, Molina CA, Rovira A, Alvarez-Sabin J, Ortega-Aznar A, Montaner J. MMP-2/MMP-9 plasma level and brain expression in cerebral amyloid angiopathy-associated hemorrhagic stroke. Brain Pathol. 2012; 22:133–141. [PubMed: 21707819]

Hsiao K, Chapman P, Nilsen S, Eckman C, Harigaya Y, Younkin S, Yang F, Cole G. Correlative memory deficits, Abeta elevation, and amyloid plaques in transgenic mice. Science. 1996; 274:99–102. [PubMed: 8810256]

Jellinger K. Alzheimer disease and cerebrovascular pathology: an update. J Neural Transm. 2002; 109:813–836. [PubMed: 12111471]

Kimchi E, Kajdasz S, Bacskai B, Hyman B. Analysis of cerebral amyloid angiopathy in a transgenic mouse model of Alzheimer disease using *in vivo* multiphoton microscopy. 2001; 60:274–279.

Kinnecom C, Lev M, Wendell L, Smith E, Rosand J, Frosch M, Greenberg S. Course of cerebral amyloid angiopathy–related inflammation. Neurology. 2007; 68:1411–1416. [PubMed: 17452586]

Klunk WE, Bacskai BJ, Mathis CA, Kajdasz ST, McLellan ME, Frosch MP, Debnath ML, Holt DP, Wang Y, Hyman BT. Imaging Aβ Plaques in Living Transgenic Mice with Multiphoton Microscopy and Methoxy-X04, a Systemically Administered Congo Red Derivative. 2002; 61:797–805.

Lakhan SE, Kirchgessner A, Tepper D, Leonard A. Matrix metalloproteinases and blood-brain barrier disruption in acute ischemic stroke. 2013; 4

Lee J, Yin K, Hsin I, Chen S, Fryer JD, Holtzman DM, Hsu CY, Xu J. Matrix metalloproteinase-9 in cerebral-amyloid-angiopathy-related hemorrhage. J Neurol Sci. 2005; 229:249–254. [PubMed: 15760647]

Lee J, Yin K, Hsin I, Chen S, Fryer JD, Holtzman DM, Hsu CY, Xu J. Matrix metalloproteinase–9 and spontaneous hemorrhage in an animal model of cerebral amyloid angiopathy. Ann Neurol. 2003; 54:379–382. [PubMed: 12953271]

Mandybur TI. Cerebral amyloid angiopathy: the vascular pathology and complications. 1986; 45:79–90.

McColl BW, Rose N, Robson FH, Rothwell NJ, Lawrence CB. Increased brain microvascular MMP-9 and incidence of haemorrhagic transformation in obese mice after experimental stroke. 2010; 30:267–272.

Montine TJ, Phelps CH, Beach TG, Bigio EH, Cairns NJ, Dickson DW, Duyckaerts C, Frosch MP, Masliah E, Mirra SS, Nelson PT, Schneider JA, Thal DR, Trojanowski JQ, Vinters HV, Hyman BT. National Institute on Aging-Alzheimer's Association guidelines for the neuropathologic assessment of Alzheimer's disease: a practical approach. Acta Neuropathol. 2012; 123:1–11. [PubMed: 22101365]

Nagase H, Woessner JF Jr. Matrix metalloproteinases. J Biol Chem. 1999; 274:21491–21494. [PubMed: 10419448]

Nicoll JA, Wilkinson D, Holmes C, Steart P, Markham H, Weller RO. Neuropathology of human Alzheimer disease after immunization with amyloid-β peptide: a case report. Nat Med. 2003; 9:448–452. [PubMed: 12640446]

Okazaki H, Reagan TJ, Campbell RJ. Clinicopathologic studies of primary cerebral amyloid angiopathy. Mayo Clin Proc. 1979; 54:22–31. [PubMed: 759733]

Pfeifer M, Boncristiano S, Bondolfi L, Stalder A, Deller T, Staufenbiel M, Mathews PM, Jucker M. Cerebral hemorrhage after passive anti-Abeta immunotherapy. Science. 2002; 298:1379. [PubMed: 12434053]

Piazza F, Greenberg SM, Savoiardo M, Gardinetti M, Chiapparini L, Raicher I, Nitrini R, Sakaguchi H, Brioschi M, Billo G. Anti–amyloid β autoantibodies in cerebral amyloid angiopathy–related inflammation: Implications for amyloid-modifying therapies. Ann Neurol. 2013; 73:449–458. [PubMed: 23625526]

Ramos-Fernandez M, Bellolio MF, Stead LG. Matrix metalloproteinase-9 as a marker for acute ischemic stroke: a systematic review. 2011; 20:47–54.

Robbins EM, Betensky RA, Domnitz SB, Purcell SM, Garcia-Alloza M, Greenberg C, Rebeck GW, Hyman BT, Greenberg SM, Frosch MP, Bacskai BJ. Kinetics of cerebral amyloid angiopathy progression in a transgenic mouse model of Alzheimer disease. J Neurosci. 2006; 26:365–371. [PubMed: 16407531]

Seo JH, Guo S, Lok J, Navaratna D, Whalen MJ, Kim KW, Lo EH. Neurovascular matrix metalloproteinases and the blood-brain barrier. Curr Pharm Des. 2012; 18:3645–3648. [PubMed: 22574977]

Serrano-Pozo A, Muzikansky A, Gomez-Isla T, Growdon JH, Betensky RA, Frosch MP, Hyman BT. Differential relationships of reactive astrocytes and microglia to fibrillar amyloid deposits in Alzheimer disease. J Neuropathol Exp Neurol. 2013; 72:462–471. [PubMed: 23656989]

Shyong M, Lee F, Kuo P, Wu A, Cheng H, Chen S, Tung T, Tsao Y. Reduction of experimental diabetic vascular leakage by delivery of angiostatin with a recombinant adeno-associated virus vector. Mol Vis. 2007; 13:133–141. [PubMed: 17293777]

Skoch, J.; Hickey, GA.; Kajdasz, ST.; Hyman, BT.; Bacskai, BJ. Anonymous Amyloid Proteins. Springer; 2005. *In vivo* imaging of amyloid-β deposits in mouse brain with multiphoton microscopy; p. 349-363.

Stitt AW, Bhaduri T, McMullen C, Gardiner TA, Archer DB. Advanced glycation end products induce blood–retinal barrier dysfunction in normoglycemic rats. 2000; 3:380–388.

Trichonas G, Manola A, Morizane Y, Thanos A, Koufomichali X, Papakostas TD, Montezuma S, Young L, Miller JW, Gragoudas E, Vavvas D. A novel nonradioactive method to evaluate vascular barrier breakdown and leakage. Invest Ophthalmol Vis Sci. 2010; 51:1677–1682. [PubMed: 19875655]

Uyama O, Okamura N, Yanase M, Narita M, Kawabata K, Sugita M. Quantitative evaluation of vascular permeability in the gerbil brain after transient ischemia using Evans blue fluorescence. 1988; 8:282–284.

Vinters HV. Cerebral amyloid angiopathy. A critical review. Stroke. 1987; 18:311–324. [PubMed: 3551211]

Vonsattel JPG, Myers RH, Tessa Hedley-Whyte E, Ropper AH, Bird ED, Richardson EP. Cerebral amyloid angiopathy without and with cerebral hemorrhages: a comparative histological study. Ann Neurol. 1991; 30:637–649. [PubMed: 1763890]

Wang X, Mori T, Jung J, Fini ME, Lo EH. Secretion of matrix metalloproteinase-2 and-9 after mechanical trauma injury in rat cortical cultures and involvement of MAP kinase. J Neurotrauma. 2002; 19:615–625. [PubMed: 12042096]

Zhao L, Lin S, Bales KR, Gelfanova V, Koger D, Delong C, Hale J, Liu F, Hunter JM, Paul SM. Macrophage-mediated degradation of beta-amyloid via an apolipoprotein E isoform-dependent mechanism. J Neurosci. 2009; 29:3603–3612. [PubMed: 19295164]

Our manuscript “Matrix metalloproteinase 9 mediated intracerebral hemorrhage (ICH) induced by cerebral amyloid angiopathy” contains new, unpublished data describing a potentially causative role for Matrix metalloproteinase 9 (MMP-9) in regulation of cerebral amyloid angiopathy (CAA) progression and vascular integrity using both human brain tissues and mouse models. Our findings can be highlighted as below:

- Found that MMP-9 co-localized with CAA, correlated with the severity of the vascular pathology, and was detected in proximity to microbleeds by examining postmortem human brain tissues.
- Characterized a novel assay using longitudinal multi-photon microscopy and a novel tracer to visualize and quantify the magnitude and kinetics of hemorrhages in 3-dimensions in living mouse brains.
- Demonstrated that topical application of recombinant MMP-9 resulted in a time- and dose-dependent cerebral hemorrhage.
- Revealed that APP mice with significant CAA developed more extensive hemorrhages which also appeared sooner after exposure to MMP-9

Our study has assessed the role of MMP-9 in CAA-associated vascular integrity in vivo. Our results and our new assay may help to clarify the mechanisms underlying CAA associated vascular disruption and may help to identify a potential therapeutic target for CAA and CAA-associated hemorrhage prevention.

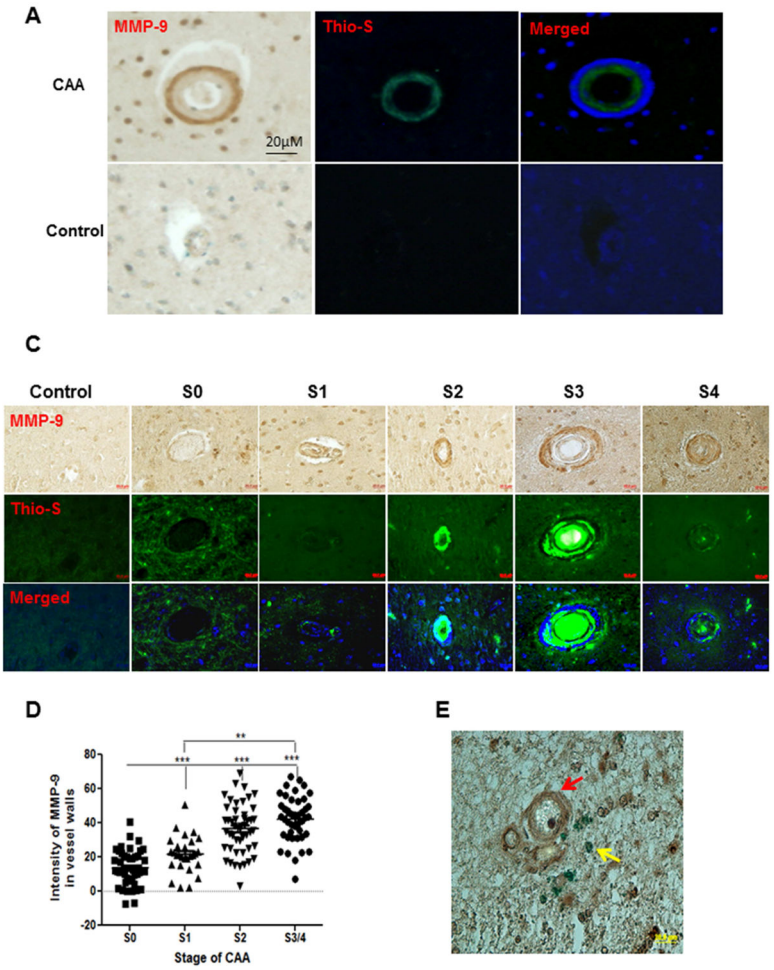

Fig. 1. MMP-9 accumulates in CAA-affected vessels

(A) Representative immunostaining of MMP-9 in brain sections from CAA patients (CAA) or control individuals (Control). Postmortem brain sections (5 μm/section, four sections per case) from the occipital lobar of CAA patients or control individuals were stained with an MMP-9 antibody recognizing the catalytic domain of MMP-9 (left panel, brown). CAA vessels were identified by thioflavin S staining (middle panel, green). The merged picture of MMP-9 staining and thioflavin S staining (right panel) shows the spatial association of MMP-9 (blue, pseudo color) and amyloid deposition (green). (B) The percentage of the thioflavin S positive vessels in total MMP-9 positive vessels. The proportion of thioflavin S positive vessels (Thio-S (+)) or thioflavin S negative vessels (Thio-S (−)) in all MMP-9 positive vessels was quantified with the CAST software. (C) Representative immunostaining of MMP-9 in CAA vessels at different stages or in control vessels. Postmortem brain sections from the occipital lobar of CAA patients or control individuals were stained with an MMP-9 antibody (upper panel, brown). CAA vessels were identified by thioflavin S staining (middle panel, green) and divided into five groups (S0, S1, S2, S3, S4) according to the grades of CAA severity as described in the Materials and Methods. The merged picture of MMP-9 staining and thioflavin S staining shows the spatial association of MMP-9 (blue, pseudo color) and amyloid deposition (green). (D) Quantitation of the MMP-9

immunoreactivity in CAA vessels at different stages or control vessels. The MMP-9 immunoreactivity of vessels was quantified by ImageJ. Vessels at stage 3 and stage 4 were combined to represent the advanced stage of CAA (S3/4). The immunoreactivity of vascular MMP-9 in brain sections from control cases were measured as the controls (Con.). *** $p < 0.001$ *vs* control. (E) Representative double staining of MMP-9 and microbleeds. Brain sections from CAA patients were double stained with an MMP-9 antibody (brown, red arrow) and Prussian blue (blue, yellow arrow) followed by imaging with a fluorescence microscope. Scale bars in A, C, E = 20 μm.

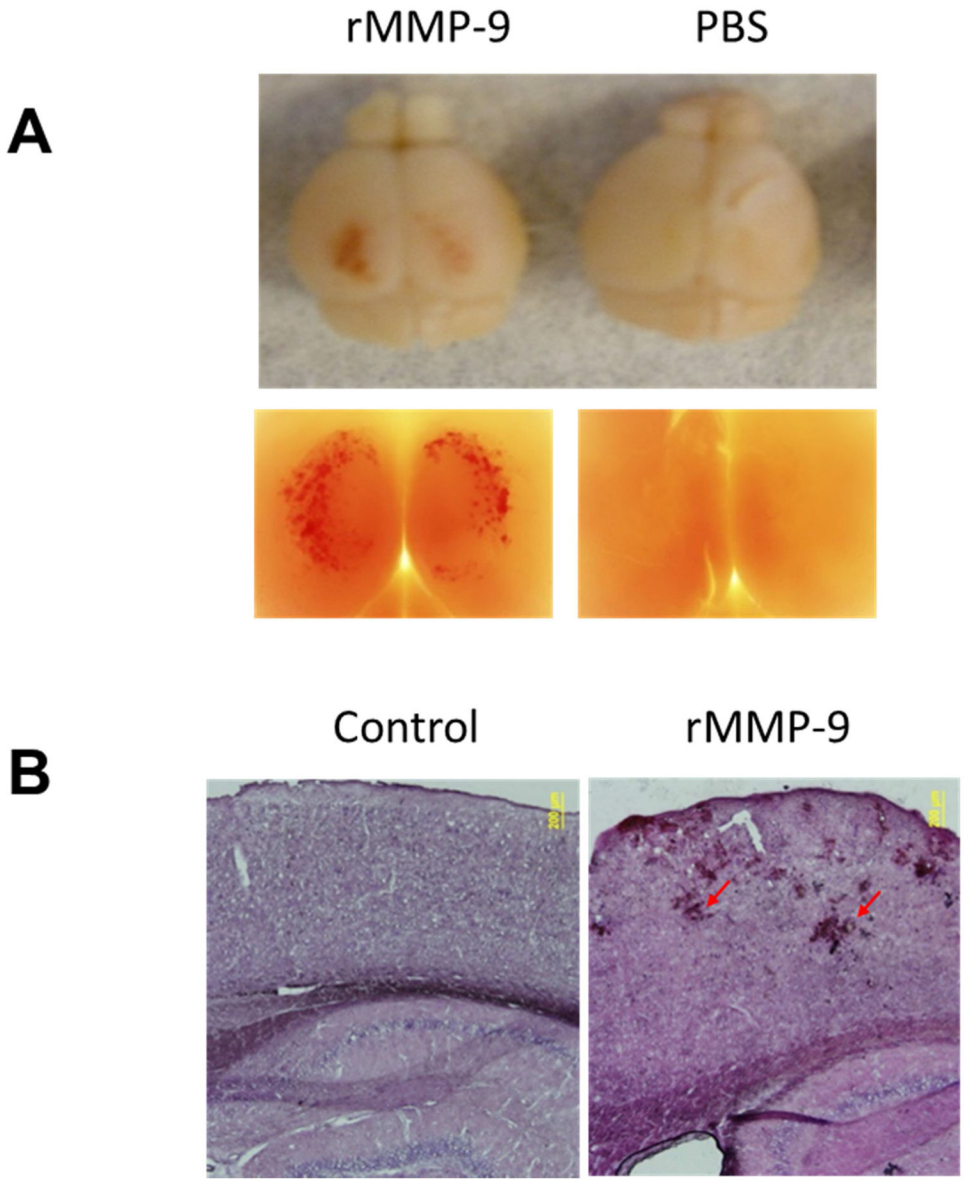

Fig. 2. Recombinant MMP-9 (rMMP-9) induces lobar hemorrhage in brains of C57/BL6 mice

(A) Representative images of mouse brains topically treated with or without rMMP-9. C57/BL6 mice at 3 months of age were prepared with a craniotomy followed by careful removal of the dura mater. Pre-activated recombinant MMP-9 (rMMP-9, 0.4 μg) or PBS (control) was topically applied to the surface of mouse brains. Forty eight hours after the treatment, the mice were sacrificed and mouse brains were removed to examine the lobar hemorrhage and imaged by a camera (upper panel) or a low magnification microscope (2.5X, Olympus) (lower panel). (B) Representative H&E staining of brain sections from mice topically treated with or without rMMP-9. Mouse brains treated with rMMP-9 or PBS (control) were sectioned and processed for histologic examination by H&E staining. Arrows show the vascular rupture in mouse brains treated with rMMP-9. Scale bar = 200 μm.

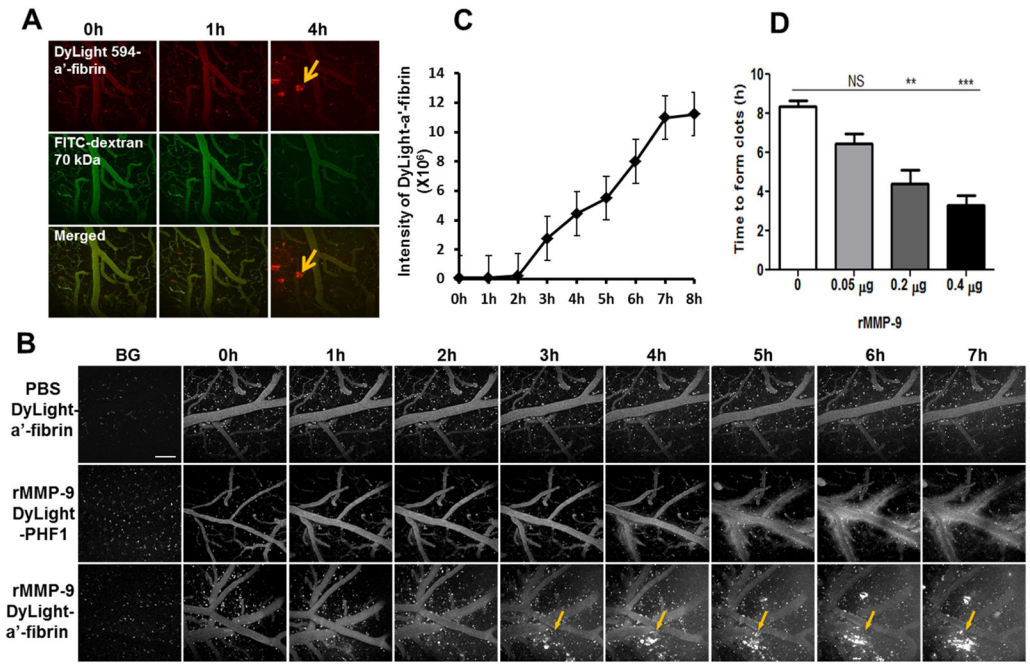

Fig. 3. Real-time visualization and quantitation of lobar hemorrhage *in vivo* by multi-photon microscopy

C57/BL6 mice, 3 months of age, were prepared with a craniotomy followed by removal of the dura mater. PBS or rMMP-9 (0.4 μg) was topically applied to the surface of mouse brains. Fluorescence-conjugated macromolecules were used as tracers. Animals were imaged hourly using a Fluoview 1000MPE Olympus multi-photon microscope to track the vascular leakage. The background images (BG) were acquired by imaging animals before administration of rMMP-9 and a tracer. (A) Examination of MMP-9-induced hemorrhage using fluorescent-anti-fibrin tracer. A mixture of a DyLight 594-conjugated anti-fibrin antibody (DyLight 594-α′-fibrin) and a fluorescein isothiocyanate-conjugated dextran (FITC-dextran, 70 kDa) was intravenously infused into tail veins of animals. Pre-activated rMMP-9 (0.4 μg) was topically applied to the surface of mouse brains followed by simultaneously imaging hourly in two channels to track the fluorescence signals of both DyLight 594-anti-fibrin (upper panel) and FITC-dextran (middle panel). The fluorescence signals of the DyLight 594-anti-fibrin or the FITC-dextran were merged to compare the detection sensitivity of the two tracers (lower panel). Arrows: fluorescent clots recognized by the fluorescent-anti-fibrin tracer. Scale bar = 100 μm. (B) The specificity of the fluorescent-anti-fibrin tracer in detecting of rMMP-9-induced lobar hemorrhage. Mice treated with 0.4 μg of rMMP-9 (middle and lower panels) or PBS (upper panel) were processed for hemorrhage assessment. DyLight 594-anti-fibrin (DyLight-a′-fibrin, upper and middle panels) or DyLight 594-conjuaged PHF1 antibody (DyLight-PHF1, lower panel) was used as a tracer. Arrows showing the fluorescent clots recognized by DyLight 594-a′-fibrin. Scale bar = 100 μm. (C) The volume of hemorrhage was determined by quantifying the fluorescence intensity of DyLight 594-anti-fibrin that accumulated at the clots. (D) Effects of different doses of rMMP-9 on hemorrhage induction. PBS (0 μg of rMMP-9) or rMMP-9 at dose of 0.05 μg, 0.2 μg, or 0.4 μg were topically applied to the mouse brains. Mice were

processed for imaging hourly up to 7 hours of time period. DyLight 594-anti-fibrin was used as a tracer. The time that the clots were first detected (time to form clots) was measured. NS = not significant; ** $p < 0.01$; *** $p < 0.001$ *vs* PBS treatment (0 μg). $n = 3 – 5$.

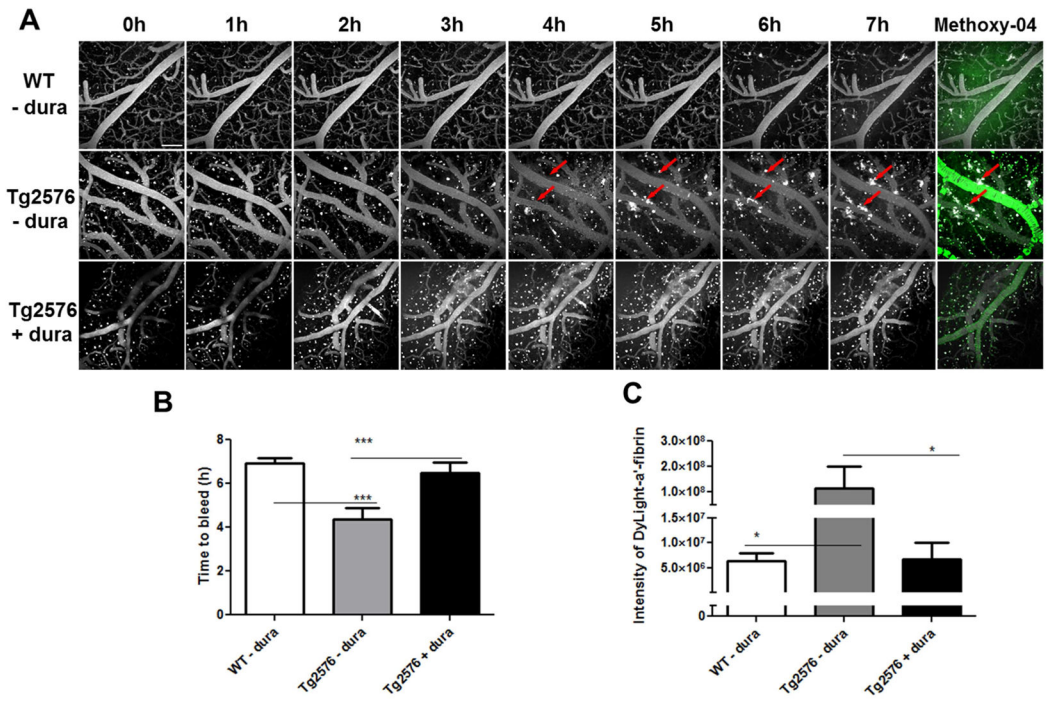

Fig. 4. MMP-9 induces an earlier onset and a greater magnitude of hemorrhage in Tg2576 mice compared to age-matched littermates

(A) Hemorrhage induction of rMMP-9 in old Tg2576 mice. Tg2576 mice or their age-matched nontransgenic littermates, 15 months of age, were prepared with a craniotomy followed by removal of the dura mater. rMMP-9 (0.05 μg) was topically applied to brain surface of Tg2576 mice (Tg2576 − dura) or their age-matched nontransgenic littermates (WT - dura). Tg2576 mice that the dura mater was removed on the right hemispheres whereas the dura mater preserved on the left hemispheres were treated in parallel as a procedure control (Tg2576 + dura). Fluorescent-anti-fibrin was injected into mice via tail vein followed by imaging hourly up to 7 hours. Thirty minutes before imaging at 7 hour time point, 300 μl of methoxy-X04 was intraperitoneally injected into the animal to label CAA affected vessels (green). Arrows show the fluorescent clots recognized by fluorescent-anti-fibrin. Scale bar = 100 μm. (B) The time points that the clots were first detected within mouse brains (Time to bleed) were measured and compared. (C) The fluorescence intensity of fluorescent-anti-fibrin in sum intensity projection of stacks were measured and analyzed by ImageJ software. * $p < 0.05$; *** $p < 0.001$ *vs* Tg2576 mice with dura removed. $n = 3 – 5$.

Table 1

Characteristics of control and CAA subjects examined in this study

Case ID	Age	Gender	AD[a]	CAA	Group
1248	63	M	A3B3C3	Severe	AD+CAA
1023	88	M	A3B3C3	Severe	AD+CAA
1186	85	M	A3B3C3	Severe	AD+CAA
919	82	M	A3B3C3	Moderate	AD+CAA
1150	66	F	A1B2C1	Severe	CAA
821	89	M	A1B1C1	Severe	CAA
1138	75	F	A0B0C0	Severe	CAA
458	80	M	A0B1C0	Severe	CAA
753	77	F	A1B1C1	Severe	CAA
960	68	M	A1B1C1	Moderate	CAA
287	66	M	A0B0C0	Mild	Control
873	74	F	A1B1C0	Absent	Control
792	71	M	A0B0C0	Absent	Control
326	>90	M	A1B1C0	Absent	Control
373	80	F	A1B1C0	Absent	Control

[a]The ABC scoring scheme (Montine et al., 2012): the A represents the assessment of Amyloid burden (by the modified Thal scoring scheme); the B represents the Braak stage (consolidated from 6 tiers to 3) and the C represents the neuritic plaque score.